UNIVERSITY OF HELSINKI REPORT SERIES IN PHYSICS

HU-P-D246

SPECTROSCOPIC PROPERTIES OF MATERIALS USING ELECTRONIC-STRUCTURE CALCULATIONS

Jaakko Koskelo

Division of Materials Physics
Department of Physics
Faculty of Science
University of Helsinki
Helsinki, Finland

ACADEMIC DISSERTATION

To be presented, with the permission of
the Faculty of Science of the University of Helsinki,
for public criticism in Auditorium XII
of the main building of the University of Helsinki, Unioninkatu 34,
on 3rd of December 2016 at 10 o'clock AM.

Helsinki 2016

Supervisor

Dr. Mikko Hakala
Department of Physics
University of Helsinki
Helsinki, Finland

Pre-examiners

Dr. Bernardo Barbiellini
Department of Physics
Northeastern University
Boston, USA

Prof. Silvana Botti
Institute of Condensed Matter Physics and Solid State Optics
Friedrich-Schiller University of Jena
Jena, Germany

Opponent

Prof. Patrick Rinke
Department of Applied Physics
Aalto University
Espoo, Finland

Custos

Prof. Keijo Hämäläinen
Department of Physics
University of Helsinki
Helsinki, Finland

Report Series in Physics HU-P-D246
ISSN 0356-0961
ISBN 978-951-51-2230-8 (printed version)
ISBN 978-951-51-2231-5 (pdf version)
http://ethesis.helsinki.fi/
Unigrafia Oy
Helsinki 2016

Preface

The research in this thesis was conducted at the Department of Physics at the University of Helsinki. I am thankful for the previous and current head of the department, Prof. Juhani Keinonen and Prof. Hannu Koskinen, for the opportunity to work here. I wish to thank Väisälä Foundation and MATRENA Doctoral Programme for the funding for the thesis work.

I wish to thank my supervising professor Keijo Hämäläinen for his support and encouragement, and for finding me time despite of his very busy schedule. I am very grateful for Dr. Mikko Hakala who was my main instructor, and provided a huge amount of guidance and support through these years. Dr. Simo Huotari acted as third, unofficial, supervisor, and I appreciate much his help and guidance. From the HELIXS group, I am thankful for Dr. Javad Hashemi, Dr. Iina Juurinen, Dr. Johannes Niskanen, Dr. Susi Lehtola, Dr. Ali Akbari, and Dr. Kari Ruotsalainen for many helpful discussions. I would like to especially mention Iina and Javad, my office mates. In addition to important contributions for this thesis, I very much enjoyed the informal discussions and company in the shared offices. I also learned a lot from the work conducted with Johannes, and benefitted from his eagerness to explain many concepts in x-ray spectroscopy and physics in general.

I have been lucky to collaborate with many accomplished and nice people, and their input has been invaluable for this thesis. I am thankful for Dr. Matthew McGrath and Prof. I-Feng Kuo for the ionic liquid molecular dynamics simulations, and useful discussions on these. I thank Dr. Giorgia Fugallo, Dr. Matteo Gatti, Dr. Pierluigi Cudazzo, and Dr. Francesco Sottile for a great collaboration, and for their hospitality during my visits in Paris.

It has been a pleasure to work at the x-ray laboratory, and I want to thank all the members for creating the nice athmosphere. I want to thank them for the weekly recreational activities, floorball, futsal, and board games, and especially Patrik Ahvenainen for organizing these events.

Finally, I would like thank my family for all the support during these years, and encouragement for science studies.

J. Koskelo: Spectroscopic properties of materials using electronic-structure calculations, University of Helsinki, 2016, 42 pages + appendices. University of Helsinki, Report Series in Physics, HU-P-D246.

Keywords: electronic structure, density-functional theory, Bethe-Salpeter equation, exciton, intermediate-band solar cell, spectroscopy, Compton profile, inelastic x-ray scattering, optical absorption

Abstract

The response of materials to electromagnetic radiation is important for two reasons: it is crucial for many applications and can also be used to study the microscopic and electronic structure that determine other properties of materials. Calculations on the quantum-mechanical state of the electrons, the electronic structure, are useful for interpreting the results of experiments where materials are probed by electromagnetic radiation. This thesis consists of three studies where electronic-structure calculations have been employed in investigating materials and their response to electromagnetic radiation. In the first paper, x-ray Compton-profile difference between solid and liquid phases of ionic liquid [mmim]Cl is calculated. The structural changes that affect this Compton-profile difference are analyzed. In the second paper, the dopant configuration and band structure of an intermediate-band solar-cell material Fe-doped $CuGaS_2$ is studied, along with optical absorption spectra. In the third paper, excitons in layered materials are investigated using a hexagonal boron nitride as an example material, and the connection between bulk and monolayer excitons is discussed. These studies provide a view on the possibilities of electronic-structure calculations for understanding the spectroscopic properties of materials from atomic and electronic level.

List of papers

This thesis consists of an introductory part and three research articles, which are referred to by the Roman numerals **I**–**III** throughout the text.

I J. Koskelo, I. Juurinen, K. O. Ruotsalainen, M. J. McGrath, I-F. Kuo, S. Lehtola, S. Galambosi, K. Hämäläinen, S. Huotari, and M. Hakala, *Intra- and intermolecular effects on the Compton profile of the ionic liquid 1,3-dimethylimidazolium chloride*, J. Chem. Phys. **141**, 244505 (2014).

II J. Koskelo, J. Hashemi, S. Huotari, and M. Hakala, *First-principles analysis of the intermediate band in* $CuGa_{1-x}Fe_xS_2$, Phys. Rev. B **93**, 165204 (2016).

III J. Koskelo, G. Fugallo, M. Hakala, M. Gatti, F. Sottile, and P. Cudazzo, *Excitons in van der Waals materials: from monolayer to bulk hexagonal boron nitride*, submitted to Phys. Rev. B.

The papers **I-III** are included as appendices.

Author's (J.K.) contribution

The author performed the Compton-profile calculations and numerical analysis of the results in paper **I**, as well as wrote the first version of the manuscript. The author performed the calculations and wrote the first version of manuscript in paper **II**. The author performed numerical BSE calculations in paper **III** (excluding the GW corrections and the monolayer case) and participated to the analysis of the results and wrote first version of parts of the manuscript related to these calculations.

Related work

List of work by the author that is closely related to this thesis but not included in it:

1. I. Juurinen, S. Galambosi, A. G. Anghelescu-Hakala, J. Koskelo, V. Honkimäki, K. Hämäläinen, S. Huotari, and M. Hakala, *Molecular-Level Changes of Aqueous Poly(N-isopropylacrylamide) in Phase Transition*, J. Phys. Chem. B **118**, 5518 (2014).

2. J. Niskanen, C. J. Sahle, I. Juurinen, J. Koskelo, S. Lehtola, R. Verbeni, H. Müller, M. Hakala, and S. Huotari, *Protonation Dynamics and Hydrogen Bonding in Aqueous Sulfuric Acid*, J. Phys. Chem. B **119**, 11732 (2015).

3. G. Fugallo, M. Aramini, J. Koskelo, K. Watanabe, T. Taniguchi, M. Hakala, S. Huotari, M. Gatti, and F. Sottile, *Exciton energy-momentum map of hexagonal boron nitride*, Phys. Rev. B **92**, 165122 (2015).

4. J. Niskanen, K. Kooser, J. Koskelo, T. Käämbre, K. Kunnus, A. Pietzsch, W. Quevedo, M. Hakala, A. Föhlisch, S. Huotari, E. Kukk, *Density functional simulation of resonant inelastic X-ray scattering in liquids: acetonitrile*, Phys. Chem. Chem. Phys. **18**, 26026 (2016).

Contents

1 Introduction

Materials physics seeks to understand and manipulate materials' properties based on the theories and methods of physics. Various spectroscopies constitute an important class of methods to study materials. Spectroscopy can be considered as the study of materials' response as a function of energy of the probe or excitations that are occurrences of states higher in energy than the thermodynamically minimum one. This thesis is related to spectroscopies in which the material is probed with photons, quanta of light. As spectroscopies are intimately linked to excitations, determining the state of electrons, *i.e.* the electronic structure, is crucial for the evaluation of materials' spectral response.

Electronic-structure calculations can be classified in roughly two categories. First, there are semiempirical methods in which the hamiltonian of the system depends on material-dependent parameters that can be chosen to reproduce experimental results or the parameters are varied to study different phenomena. One example of this is the empirical tight-binding method, where the so-called hopping integral is determined from experimental data. Another example is the crystal field theory with empirically determined crystal field splittings. Methods of this kind can be invaluable in explaining experimental results and gaining understanding of materials; however, the use of system-dependent parameters weaken their predictive power. As the second type, there are methods that do not take in any material-dependent parameters, but everything is calculated from the underlying theory - including approximations that are necessary to make the computations feasible. These methods are referred to as "first principles". The calculations of this type are in the focus of this thesis.

First-principles electronic-structure calculations can be used in many different ways in materials science. Perhaps most commonly their use is related to total energies and forces of atomic configurations. This includes, for example, determination of defect formation energies, predicting new stable phases of compounds, or calculation of atomic trajectories using molecular dynamics. In this thesis total energy and force calculations are used as well, mainly to generate atomic structures for subsequent calculations.

The main theme of this thesis is the calculation of spectra from electronic structure and their use to answer various questions. As the photoabsorption is an essential step in the operation of photovoltaics, solar-cell materials are a natural application domain for spectroscopy. In paper **II** the structural, electronic, magnetic and optical properties of an intermediate-band (IB) solar-cell material $CuGa_{1-x}S_2Fe_x$ are studied. In IB materials additional electronic states are engineered in the band gap of the host semiconductor, and they are one way to boost the efficiency of photovoltaics.

Spectroscopy can be used to indirectly obtain information on molecular-level geometries by comparing calculated and experimental results. Along that line, paper **I** provides a theoretical prediction for the change of the Compton profile of an ionic

liquid in solid-liquid phase transition. Furthermore, the effect of different structural motifs on the Compton profile is analyzed. Compton profiles can be measured using x-ray Compton scattering at synchrotron radiation facilities.

Materials can exhibit a wealth of different excitations, and in this thesis the most relevant elementary excitations are excitons and plasmons. Excitons can be depicted as interacting pairs of electron and electron hole (absence of electron), and they have profound effects on the optical properties of materials. Plasmons, on the other hand, are collective excitations of electron charge density. These excitations can be characterized by their dispersion relation, *i.e.*, the dependence of the excitation energy on the momentum. In paper **III** the evolution of the exciton dispersion from bulk to two-dimensional layers is investigated in hexagonal boron nitride, which is a prototypical layered insulator. Changing the interlayer distance modifies the interlayer hopping, which can be used in the analysis of excitons in layered materials. These kind of materials are currently studied a lot due to the possibility to use them for electronic devices, and exciton properties are very important for optoelectronic applications.

In the next chapter 2 the basic theoretical background and methods used in this thesis to calculate the electronic structure are discussed. In chapter 3 the relevant spectroscopies and their relation to quantities that can be obtained with methods introduced in chapter 2 are presented. The studied materials with the backgrounds and questions investigated in individual papers are introduced in chapter 4. The results are presented in chapter 5, and chapter 6 concludes the thesis.

2 Electronic-structure theory and calculations

2.1 Interacting electron system

This subsection provides the basic background and introduction to concepts of electronic structure theory[1] [1,2]. The main equation behind most of the electronic structure theory is the quantum-mechanical equation of motion, the Schödinger equation, which in its time-independent form reads

$$\mathcal{H}\Psi(\mathbf{x}_1, ..., \mathbf{x}_N; \mathbf{X}_1, ..., \mathbf{X}_K) = \mathcal{E}\Psi(\mathbf{x}_1, ..., \mathbf{x}_N; \mathbf{X}_1, ..., \mathbf{X}_K), \tag{1}$$

for a collection of N electrons and K nuclei whose internal structure is neglected. $\mathcal{H}$ is the hamiltonian, $\mathcal{E}$ the total energy, and $\Psi(\mathbf{x}_1, ..., \mathbf{x}_N; \mathbf{X}_1, ..., \mathbf{X}_K)$ the wavefunction, while $\mathbf{x}_i$ and $\mathbf{X}_j$ are the coordinates for ith and jth electron and nucleus, respectively. The coordinates include both spatial and spin degrees of freedom. The lowest energy solution for this equation is the ground-state, the rest are excited states. In the Born-Oppenheimer approximation (BOA) the electron and nuclear motions are decoupled, and the wavefunction is a product of electron and nuclear wavefunctions. The electron wavefunction depends on the nuclear positions, but not on their momenta. This decoupling can be justified by the different masses of electrons and nuclei, which often results in different time-scales for the motion of these particles. BOA is in many cases a valid approximation, and it is the basis for most of the *ab initio* calculations. It leads to an electronic Schrödinger equation

$$H\Phi(\mathbf{x}_1, ..., \mathbf{x}_N) = E\Phi(\mathbf{x}_1, ..., \mathbf{x}_N), \tag{2}$$

where H is the hamiltonian with fixed nuclear positions, Φ is the wavefunction for the electron system. E can be considered as the total energy in the presence of static nuclear point charges and it gives a potential energy for the motion of nuclei. Solving equation (2) still poses considerable difficulties, and it can be solved analytically only for the simplest cases, such as hydrogen atom. The root for these difficulties is the electron-electron interaction in the hamiltonian, which is given by the electrostatic Coulomb energy $\sum_i \sum_{j \neq i} 1/|\mathbf{r}_i - \mathbf{r}_j|$, where $\mathbf{r}_i$ is the position of the ith electron. To solve equation (2) for a system of many electrons, one has to resort to approximations and solve equations numerically. The Hartree-Fock (HF) method is one often used approximation, and in that the wavefunction is written as an antisymmetrized product of single-particle wavefunctions. The antisymmetrization is done to satisfy the exchange symmetry for identical fermions, which states that the wavefunction changes sign by

[1] Throughout this thesis the equations are given in Hartree atomic units. In these units $\hbar = m_e = e = \frac{1}{4\pi\epsilon_0} = 1$ and $c = 1/\alpha$. $\hbar$ is the reduced Planck constant, m_e the mass of electron, e the elementary charge, c the speed of light, ϵ_0 the permittivity of the vacuum, and α the fine structure constant.

exchange of two particles. The many-body wavefunction in HF method is known as the Slater determinant, and reads

$$\Phi(\mathbf{x}_1, ..., \mathbf{x}_N) = \frac{1}{\sqrt{N}} \begin{vmatrix} \phi_1(\mathbf{x}_1) & \dots & \phi_N(\mathbf{x}_1) \\ \vdots & \ddots & \vdots \\ \phi_1(\mathbf{x}_N) & \dots & \phi_N(\mathbf{x}_N) \end{vmatrix}, \tag{3}$$

where $\phi(\mathbf{x})$ are single-particle wavefunctions. HF gives the optimal wavefunction of the form (3) in a way that it minimizes the total energy

$$E = \int \mathrm{d}\mathbf{x}_1 ... \mathrm{d}\mathbf{x}_N \left|\Phi(\mathbf{x}_1, ..., \mathbf{x}_N)\right|^2 H(\mathbf{x}_1, ..., \mathbf{x}_N). \tag{4}$$

This leads to the following Schrödinger-like equation, known as the HF equation, for each single-particle wavefunction $\phi_i(\mathbf{x})$:

$$\Big\{-\frac{\nabla^2}{2} - \sum_I \frac{Z_I}{|\mathbf{r}-\mathbf{R}_I|} + \sum_j \int \mathrm{d}\mathbf{x}' \frac{|\phi_j(\mathbf{x}')|^2}{|\mathbf{r}-\mathbf{r}'|}\Big\}\phi_i(\mathbf{x}) - \sum_j \int \mathrm{d}\mathbf{x}' \frac{\phi_j(\mathbf{x})\phi_j(\mathbf{x}')}{|\mathbf{r}-\mathbf{r}'|}\phi_i(\mathbf{x}') = \varepsilon_i \phi_i(\mathbf{x}). \tag{5}$$

Z_I is the charge of the Ith nucleus and $\mathbf{R}_I$ the corresponding position. The left-hand side consists of an effective hamiltonian acting on ϕ_i, and ε_i on the right-hand side is the ith single-particle eigenenergy. The single-particle wavefunctions are hereafter also referred as orbitals. The HF equation has infinitely many solutions, and usually one chooses the N lowest-eigenenergy orbitals to be included in the Slater determinant (3). The first term in the effective hamiltonian is the kinetic energy, the second the interaction of the electron with nuclei, and third the Hartree term that describes the electrostatic interaction with the charge density of all electrons. The last term in the effective hamiltonian is the exchange interaction that rises from the wavefunction antisymmetry requirement. The interaction of electron with its own charge density in Hartree term is cancelled by the corresponding contribution in the exchange interaction. In other words, HF is free of one-particle self-interaction error.

In an interacting electron system the electrons are correlated, which means that the probability of finding electrons at coordinates $\mathbf{x}$ and $\mathbf{x}'$ is different than independently finding an electron at $\mathbf{x}$ and at $\mathbf{x}'$. In more mathematical terms, the measure of correlation can be taken as $\Delta n(\mathbf{x}, \mathbf{x}') = n(\mathbf{x}, \mathbf{x}') - n(\mathbf{x})n(\mathbf{x}')$, where $n(\mathbf{x})$ is the electron density that gives the probability to find an electron at $\mathbf{x}$. Correspondingly, $n(\mathbf{x}, \mathbf{x}')$ is the probability to find electrons at both $\mathbf{x}$ and $\mathbf{x}'$. HF accounts for correlation effects in the sense that it satisfies the Pauli exclusion principle, and consequently electrons of like spin cannot occupy the same point in space. Usually by the term "electron correlation" one refers to correlation effects beyond exchange (that is fully accounted in HF). Correspondingly, $\Delta n(\mathbf{x}, \mathbf{x}')$ is called exchange-correlation hole, and "correlation energy" is the difference between HF and exact total energies.

HF is an example of a mean-field theory, where the interaction of an electron with other electrons is taken into account by considering the average field created by the other electrons. In mean-field theories the equations are usually solved using the self-consistent-field (SCF) method. In that case, one starts with a set of orbitals, and calculates the effective hamiltonian. Next, one calculates new orbitals from the HF equation, and after this, a new effective hamiltonian. This procedure is repeated until the wavefunction, energy, or another quantity of interest does not change considerably, that is, the solution is self consistent.

The symmetries of the spatial arrangement of the atoms manifest in the single- and many-particle wavefunctions. In the case of a crystal with perfect translational symmetry, the eigenfunctions of the effective single-particle hamiltonian take the form of a Bloch function:

$$\phi_{n\mathbf{k}}(\mathbf{r}) = \mathrm{e}^{i\mathbf{k}\cdot\mathbf{r}} u_{n\mathbf{k}}(\mathbf{r}). \tag{6}$$

$\mathbf{k}$ is a wavevector, n a band index, and $u_{n\mathbf{k}}(\mathbf{r})$ a unit-cell-periodic function. Bloch functions and corresponding eigenvalues are periodic with respect to reciprocal lattice vectors. Although Bloch's theorem is usually used in the context of single-particle wavefunctions, one can similarly associate a Bloch wavevector for the many-body wavefunction, since the full many-body hamiltonian for a perfect crystal is invariant under simultaneous translation of all spatial coordinates with a lattice vector.

Single-particle models are in many cases very successful. On qualitative level, these provide a simple and intuitive picture that can be very useful for gaining insight and discussing many properties of materials. The single-particle energy levels are often used in qualitative discussion of spectra; in HF the single-particle eigenenergies can be considered as approximate electron removal or addition energies, as stated in Koopman's theorem. But often to obtain quantitative, or sometimes even qualitative, results in agreement with experiments, one has to treat electron correlation on a higher level. There are many ways to improve on HF, and a natural extension is to express the wavefunction with several Slater determinants. In fact, if a complete set of single-particle wavefunctions is used, the many-body wavefunction can be obtained exactly using a configuration interaction expansion, where a linear combination of all possible Slater determinants formed from the set of single-particle wavefunctions is considered. Instead of the many-particle wavefunction, one can alternatively work with functions that depend on smaller number of coordinates to evaluate physical observables. The next two subsections discuss such methods, namely density-functional theory and Green's function many-body theory.

2.2 Density-functional theory

Density-functional theory (DFT) [3–5] approaches the electronic-structure problem by treating the electron density $n(\mathbf{r})$ as the core variable. The rigorous theoretical foundation for DFT lies in the Hohenberg-Kohn (HK) theorems [3]. The first HK theorem states that the external potential (usually the potential of nuclei) acting on the electron system is uniquely determined by the ground-state electron density. This means that all the properties of the electron system are determined by the ground-state electron density, since all these properties can be obtained by solving the Scrödinger equation that is completely determined by the external potential. The second HK theorem introduces a universal functional $F[n]$ so that the energy $E[n] = F[n] + \int \mathrm{d}\mathbf{r} n(\mathbf{r}) V_{ext}(\mathbf{r})$ is minimized by the ground-state density, and is the ground-state energy for the given external potential $V_{ext}(\mathbf{r})$. A physically intuitive definition for the energy can be given by the constrained-search approach [6]: $E[n] = \min_{\Phi} \langle \Phi | H | \Phi \rangle$, where the minimization is done over all possible wavefunctions that give density n.

The rise of DFT to its present popularity is mostly due to development of the Kohn-Sham (KS) method [7]. KS DFT is used in all of the papers included in this thesis. In the KS method the density functional problem is mapped to an effective single-particle one. One makes an ansatz that for each density there exists a non-interacting single-particle system with the same density. The total energy is then partitioned in different contributions:

$$E[n] = T_s[n] + V_H[n] + V_{ext}[n] + E_{xc}[n], \tag{7}$$

where $T_s[n]$ is the of kinetic energy of the non-interacting system, $V_H[n]$ Hartree energy, and $V_{ext}[n]$ the Coulomb energy between charge density and external potential. The leftover term $E_{xc}[n]$ is the exchange-correlation (XC) energy, and it takes into account the exchange and correlation effects discussed in previous subsection. Minimizing the total energy leads to KS equations

$$\Big\{ -\frac{\nabla^2}{2} + V_H(\mathbf{r}) + V_{ext}(\mathbf{r}) + V_{xc}(\mathbf{r}) \Big\} \phi_i(\mathbf{r}) = \varepsilon_i \phi_i(\mathbf{r}), \tag{8}$$

where the potential terms are understood as the functional derivatives of the corresponding terms in equation (7). The electron density is given as a sum over N lowest-eigenenergy KS orbitals: $n(\mathbf{r}) = \sum_i |\phi_i(\mathbf{r})|^2$.

DFT can be formulated using only the total electron density $n(\mathbf{r})$ as above, which implicitly includes all the spin effects as well. However, in most of the practical calculations performed nowadays, DFT is formulated in a way that $n(\mathbf{r})$ is split to spin-up and spin-down components: $n(\mathbf{r}) = n_\uparrow(\mathbf{r}) + n_\downarrow(\mathbf{r})$. This leads to own XC potentials and KS orbitals for each spin.

Although the KS single-particle wavefunctions are in principle only auxiliary func-

tions that give ground-state density[2], they are still often used in practical calculations as approximate single-particle wavefunctions and their eigenenergies as approximate excitation energies. That is also the case in this thesis. The fundamental band gap $E_{fg}(N) = E(N+1) + E(N-1) - 2E(N)$ can be obtained exactly as a property of ground-state total energies. Within KS theory, it can be written as $\varepsilon_{N+1}(N+1) - \varepsilon_N(N) = \varepsilon_{N+1}(N) - \varepsilon_N(N) + \Delta_{xc}(N)$, where the value in brackets denotes the number of the electrons in the system and $\Delta_{xc}(N)$ is the change in the XC potential when one electron is added[3]. This illustrates that the band gap is not correctly given as the KS eigenenergy difference even if the exact functional is used.

A major issue in KS DFT is that the XC potential is not known. There exist a vast amount of different approximations to it. In the local density approximations (LDA) the energy density depends only on the density in the given position, and not on the density in all space. In generalized gradient approximations (GGA) also the gradient of the density is used in the parametrization. When the XC potential is approximated, DFT can suffer from the one-particle self-interaction error, because the interaction with the electron with its own charge density in the Hartree term is not fully cancelled by approximate exchange energy.

2.2.1 Hybrid exchange-correlation functionals

Hybrid XC functionals have been developed to alleviate some shortcomings of standard semilocal[4] XC functionals. In hybrid functionals one mixes the exact exchange energy from HF method with the semilocal XC functional. Usually one uses the non-local HF-like exchange term in the single-particle equation, instead of the local potential that is defined as the functional derivative with respect to density[5], and consequently one does not work within the standard KS theory. Non-local potentials can, however, be treated rigorously in the density-functional framework by using the generalized Kohn-Sham (GKS) theory [9].

Due to the non-local exchange, part of Δ_{xc} can be included in the orbital eigenenergies, and hybrid functionals often lead to significant improvements in band gap compared to usual semilocal functionals. The better agreement on band-gap energies can also be explained with empirical arguments: HF tends to overestimate band gaps, while

[2]The only exception is the highest occupied KS orbital whose eigenenergy gives the exact ionization potential for finite system [8].

[3]Strictly speaking, Δ_{xc} can be interpreted as the change in XC potential alone only when there is a very large number of electrons, in which case the change in the density and orbitals is infinitesimal upon electron addition.

[4]Semilocal refers to the fact that the energy density depends only on the density and its gradient in the given position.

[5]The exact exchange could alternatively be treated using optimized effective potential (OEP) method, which gives a local potential. The basic idea in OEP is to use the chain rule of functional derivatives to calculate the functional derivative of an orbital-dependent energy with respect to density.

KS DFT underestimates these when the band gap is calculated from orbital eigenenergies neglecting Δ_{xc}. Also total energies and related properties, like bond lengths, are often improved compared to semilocal functionals. Often hybrid functionals provide a reasonable compromise between accuracy and computational speed, and can be used to obtain good description of structural and electronic properties simultaneously.

The fractional mixing of exact exchange into density functional can be rationalized [10, 11] using adiabatic connection, where one continuously switches from non-interacting to interacting electron system keeping the density fixed to the one of the interacting system. The XC energy is obtained by integrating XC potential energy over a coupling constant that gives the strength of the electron-electron Coulomb repulsion. Arguments based on this approach have lead [11] to the often used 1/4 mixing of exact exchange with the exchange of semilocal functional. Another physically well motivated way to choose the mixing fraction would be to use connection to linear-response many-body theory. The single-particle equation for a non-local hybrid functional bears resemblance to the quasiparticle equation introduced in the next subsection. By comparison with the Coulomb hole and screened exchange (COHSEX) approximation [12], one can motivate the choice $1/\epsilon_0$ for the mixing fraction [13, 14], where ϵ_0 is the static dielectric constant.

HF can be problematic in solids for two reasons. First, taking the exact exchange into account in large system can be computationally intensive, at least compared to standard DFT. Second, HF fails in metals giving a vanishing density of states at Fermi level. These issues follow to hybrid functionals where the exact exchange with the full-range Coulomb potential is mixed with the local exchange potential. Nevertheless, both of these can be alleviated by keeping only the short-range part of the exact exchange. This can be done, for example, by decomposing the Coulomb interaction using error function and its complementary counterpart: $1/r = \frac{\mathrm{erfc}(\mu r)}{r} + \frac{\mathrm{erf}(\mu r)}{r}$, as is done in the popular HSE functional [15, 16]. Here, μ is a parameter that determines the partition into short- and long-range contributions. The short-ranged nature of the exact exchange in HSE functional allows one to use a coarser $\mathbf{k}$ grid for constructing the exchange interaction operator [17].

In this thesis, HSE hybrid functional is used in paper **II** to study the band structure and ground-state energetics of intermediate-band solar-cell material Fe-doped $CuGaS_2$.

2.3 Green's function many-body theory

The interacting many-particle problem can alternatively be formulated using Green's functions (propagators) [18–22]. One can then avoid solving the many-coordinate wavefunction, and work with functions of lesser number of coordinates. Of course, it depends on the problem and system at hand which of these approaches leads to more tractable calculations with sufficient accuracy. Compared to the (time-independent)

DFT, Green's functions provide more direct access to excited-state properties. Also, it can provide a more systematic and hierarchical way to obtain ground-state properties. In this thesis, methods based on Green's functions are used in paper **III** to obtain electronic excitations and dielectric properties in a layered material.

The one- and two-particle Green's functions are defined as

$$G(\mathbf{x}t, \mathbf{x}'t') = -i\langle N|T[\hat{\phi}(\mathbf{x}, t)\hat{\phi}^\dagger(\mathbf{x}', t')]|N\rangle, \tag{9}$$

$$G(\mathbf{x}_1t_1, \mathbf{x}_2t_2, \mathbf{x}_1't_1', \mathbf{x}_2't_2') = -\langle N|T[\hat{\phi}(\mathbf{x}_1, t_1)\hat{\phi}(\mathbf{x}_2, t_2)\hat{\phi}^\dagger(\mathbf{x}_2', t_2')\hat{\phi}^\dagger(\mathbf{x}_1', t_1')]|N\rangle. \tag{10}$$

$|N\rangle$ is an N-particle ground state in the second quantization formalism, and $\hat{\phi}(\mathbf{x}, t)$ ($\hat{\phi}^\dagger(\mathbf{x}, t)$) is an electron field operator in the Heisenberg picture that destroys (creates) an electron at coordinate $\mathbf{x}$ and time t. T is a time-ordering operator that puts the electron field operators in descending order in time from left to right. The one-particle Green's function gives the probability amplitude for a process where an electron is created at $(\mathbf{x}', t')$ and destroyed at $(\mathbf{x}, t)$. Depending on the ordering of t and t', it describes the propagation of either electron or hole (absence of electron). The two-particle Green's function can describe several different processes according to the values of the time variables, including the simultaneous propagation of electron and hole, which is relevant for the dielectric properties calculated in this thesis. When the hamiltonian is time-independent, the one-particle Green's function only depends on the time difference $t' - t$ and can conveniently be Fourier-transformed to energy space, where it has poles at the total energy differences between the N-particle ground state and the states of $N \pm 1$-particle systems. Correspondingly, the particle-hole Green's function, a part of the two-particle Green's function that describes the simultaneous propagation of electron and hole, has poles at charge-neutral excitation energies.

The one-particle Green's function can be obtained from an equation of motion that also involves the two-particle Green's function. Alternatively, one can obtain a Dyson-like equation for it, which takes use of the Green's function of the non-interacting system, G_0, and reads

$$G(12) = G_0(12) + \int \mathrm{d}(34) G_0(13)\Sigma(34)G(42), \tag{11}$$

where Σ is the (proper) self-energy and it takes into account the complicated many-particle effects. For brevity, a notation where coordinate $\mathbf{x}$ and time t are combined to a numeral, such that $1 = (\mathbf{x}_1, t_1)$ and $2 = (\mathbf{x}_2, t_2)$ etc., is introduced. The self-energy, and Green's function, can be obtained by treating the interparticle Coulomb potential as a perturbation, which leads to the standard diagrammatic representation of many-body theory [21,22]. One can alternatively build the theory around a screened interaction W, which is significantly weaker than the bare Coulomb potential. This

leads to Hedin's equations [12], a set of equations to be solved self-consistently, that besides the Dyson equation (11) are[6]

$$\Sigma(12) = i \int \mathrm{d}(34) G(13) \Gamma(324) W(41), \tag{12}$$

$$W(12) = v(12) + \int \mathrm{d}(34) v(13) P(34) W(42), \tag{13}$$

$$P(12) = -i \int \mathrm{d}(34) G(13) G(41) \Gamma(342), \tag{14}$$

$$\Gamma(123) = \delta(12)\delta(13) + \int \mathrm{d}(4567) \frac{\delta \Sigma(12)}{\delta G(45)} G(46) G(75) \Gamma(673). \tag{15}$$

P is the irreducible polarizability, and Γ is called the (irreducible) vertex function. By iterating these equations, one can obtain approximations for self-energy with increasing hierarchy. The first iteration yields $\Sigma(12) = G(12)W(21)$, which is referred to as the GW approximation, and is the basis for a large portion of beyond-DFT band-structure calculations performed at present day.

Sometimes the materials properties can be well described by picturing the electron system composing of weakly interacting fictitious particles, quasiparticles. These can be thought consisting of a bare particle, like electron, and the surrounding polarization cloud that is formed due to the interaction between the electrons. In the quasiparticle approximation the Green's function is

$$G(\mathbf{x}, \mathbf{x}', \omega) = \sum_i \frac{\phi_i^{QP}(\mathbf{x}) \phi_i^{QP*}(\mathbf{x}')}{\omega - E_i^{QP}}, \tag{16}$$

where $\phi_i^{QP}(\mathbf{x})$ is a quasiparticle wavefunction and E_i^{QP} a corresponding energy. The form of this equation is similar to that of the non-interacting electrons, with the exception that the energy E_i^{QP} is complex. The real part of E_i^{QP} gives the electron removal and addition energies, and imaginary part the inverse lifetime of the quasiparticle. The quasiparticle wavefunctions and energies can be obtained from the quasiparticle equation

$$H_0(\mathbf{x})\, \phi_i^{QP}(\mathbf{x}) + \int \mathrm{d}\mathbf{x}'\, \Sigma(\mathbf{x}, \mathbf{x}', E_i^{QP})\, \phi_i^{QP}(\mathbf{x}) = E_i^{QP} \phi_i^{QP}(\mathbf{x}), \tag{17}$$

where $H_0(\mathbf{x})$ is the single-particle term including kinetic energy and external and Hartree potentials.

[6]Here, the Hartree potential is taken into account in G_0 and is not part of the self-energy.

2.3.1 Bethe-Salpeter equation

The one-particle Green's function gives the excitations related to the removal and addition of electron that can be probed by direct and inverse photoemission spectroscopy, respectively. To obtain charge-neutral excitations that are relevant for dielectric properties, one also needs additional information. That could be obtained, for example, from the two-particle correlation function L, which is closely related to the two-particle Green's function: $L(1234) = iG(1423) - iG(12)G(43)$. It obeys a Dyson-like equation, the Bethe-Salpeter equation (BSE), which reads

$$L(1234) = L_0(1234) + \int \mathrm{d}(5678) L_0(1256) \left[v(57)\delta(56)\delta(78) + \frac{\delta\Sigma(56)}{\delta G(78)} \right] L(7834), \quad (18)$$

where $L_0(1234) = -iG(13)G(42)$ is the non-interacting two-particle correlation function that describes the propagation of two independent particles. If one uses the GW approximation for the self-energy and further approximates $\delta W/\delta G = 0$, one obtains

$$L(1234) = L_0(1234) + \int \mathrm{d}(5678) L_0(1256) \left[v(57)\delta(56)\delta(78) - W(56)\delta(57)\delta(68) \right] L(7834), \quad (19)$$

This approximation is known as the time-dependent screened Hartree-Fock and it forms the basis for the standard implementation of the BSE for calculations of charge-neutral excitations in real materials. The first term in the square brackets is called electron-hole (e-h) exchange interaction[7] that is responsible for the crystal local-field effects discussed in next subsection. The second term is the direct screened electron-hole (e-h) attraction, and is responsible for creating bound excitons, that is, excitons with energy smaller than the fundamental band gap. In accordance with the GW approximation for the self-energy, the screening is calculated at the level of random-phase approximation, although model dielectric functions are sometimes also employed. Additionally, the screening is assumed to be static in most practical calculations. The standard implementation of BSE furthermore uses the quasiparticle form (16) for the one-particle Green's function and the quasiparticle wavefunctions and energies are approximated to be orthonormal and real, respectively. In practice, the quasiparticle wavefunctions are often approximated by LDA wavefunctions with corresponding energies corrected by perturbative GW. If one then uses these quasiparticle wavefunctions as basis states, one obtains the following matrix form for the BSE:

[7] We now assume the time variables in L are set in a way that gives the simultaneous propagation of electron and hole.

$$L^{(n_3n_4)}_{(n_1n_2)}(\omega) = \int \mathrm{d}\mathbf{r}_1\mathrm{d}\mathbf{r}_2\mathrm{d}\mathbf{r}_3\mathrm{d}\mathbf{r}_4 L(\mathbf{r}_1,\mathbf{r}_2,\mathbf{r}_3,\mathbf{r}_4,\omega)\phi^*_{n_1}(\mathbf{r}_1)\phi_{n_2}(\mathbf{r}_2)\phi_{n_3}(\mathbf{r}_3)\phi^*_{n_4}(\mathbf{r}_4) \quad (20)$$

$$= [H_{exc} - \omega 1]^{-1\,(n_3n_4)}_{\quad\ (n_1n_2)}(f_{n_4} - f_{n_3}), \quad (21)$$

$$H_{exc\,(n_1n_2)}^{\ \ (n_3n_4)}(\omega) = (\varepsilon_2 - \varepsilon_1)\delta_{n_1,n_3}\delta_{n_2,n_4} + (f_{n_1} - f_{n_2})\left[V_{X\,(n_1n_2)}^{\ \ (n_3n_4)} - W_{D\,(n_1n_2)}^{\ \ (n_3n_4)}\right]. \quad (22)$$

H_{exc} is an effective two-particle hamiltonian, called the excitonic hamiltonian. (n_1n_2) is a composite index describing a transition between quasiparticle states n_1 and n_2 and f_{n_1} is the occupation number of quasiparticle state n_1. V_X and W_D are the exchange e-h and direct screened interactions rising from the corresponding terms in equation (19).

Only transitions between occupied (v) and unoccupied (c) states are relevant, and these transitions can be classified as resonant ($v \to c$) and antiresonant ($c \to v$). The excitonic hamiltonian can be split to four matrix blocks according to the nature of the transitions. If one neglects the blocks that couple resonant and antiresonant transitions, one obtains the Tamm-Dancoff approximation (TDA), which is also applied in the calculations in this thesis.

The matrix inversion in equation (21) can be done either by directly inverting this equation[8] or by diagonalizing the excitonic hamiltonian and then exploiting its eigenvalue decomposition for obtaining $[H_{exc} - \omega 1]^{-1}$. The inversion without diagonalization is computationally less demanding. On the other hand, the diagonalization allows a more straightforward analysis of dark and triplet excitons (see section 5.3 and paper **III**). Furthermore, it provides access to excitonic wavefunction.

2.4 Response functions and screening

Linear-response theory studies the effects of an external perturbation employing the assumption that the induced changes in the expectation values of operators are linear in the strength of the perturbation. This is a valid assumption in many spectroscopic experiments, and it holds if the strength of the radiation field is not too large. An essential quantity in the linear response of the electronic structure of materials, the density-density response function χ, is defined as

$$n_{ind}(\mathbf{r},t) = \int \mathrm{d}\mathbf{r}'\mathrm{d}t'\chi(\mathbf{r},\mathbf{r}',t-t')V_{ext}(\mathbf{r}',t'), \quad (23)$$

where n_{ind} is the electron density induced by the perturbing external potential V_{ext}. The induced electron density creates its own electrostatic potential V_{ind}. By considering the

[8] This is usually done using the Haydock scheme, where one transforms the excitonic hamiltonian into tridiagonal form to calculate the matrix elements of the resolvent $[H_{exc} - \omega\mathbb{1}]^{-1}$ using a continued fraction [23, 24].

response of the system to the total potential $V_{tot} = V_{ext} + V_{ind}$, one obtains so-called irreducible response functions. The irreducible counterpart for χ, the (irreducible) polarizability P, is then defined as

$$n_{ind}(\mathbf{r}, t) = \int \mathrm{d}\mathbf{r}'\mathrm{d}t' P(\mathbf{r}, \mathbf{r}', t - t') V_{tot}(\mathbf{r}', t'). \tag{24}$$

This is the same P that appeared before in section 2.3 in one of the Hedin's equations. Correspondingly, χ is sometimes called reducible polarizability, and it is connected to the irreducible one through a Dyson-like equation $\chi(12) = P(12) + \int \mathrm{d}(34) P(13) v(34) \chi(42)$, where the abbreviated notation has been used again. Another important identity for χ is its connection to the two-particle correlation function L, which can be be thought as a four-point generalization of the reducible polarizability: $\chi(12) = L(1122)$.

The response functions that are obtained directly through the connection to many-body perturbation theory are time ordered (see equations (9) and (10)). In contrast, the response functions that are directly related to spectroscopies are causal. Qualitatively, this can be understood as that any perturbation can lead to effects only after the perturbation has occurred, not before. Fortunately, causal response functions can simply be obtained from time-ordered ones: $R_C(\mathbf{x}_1, \mathbf{x}_2; \omega) = R_T(\mathbf{x}_1, \mathbf{x}_2; \omega)$ for $\omega > 0$ generally for any response function R. The negative-energy part of causal function can then be obtained from the positive through complex conjugation: $R_C(\mathbf{x}_1, \mathbf{x}_2; -\omega) = R_C^*(\mathbf{x}_1, \mathbf{x}_2; \omega)$. Furthermore, the real and imaginary parts of causal response functions are related to each other through the Kramers-Kronig relations.

When external potential is applied to the electron system, the electrons rearrange in a way that the total potential V_{tot} is on average weaker than V_{ext}, in other words, the potential is screened. The strength of the screening is given by the microscopic linear dielectric function ϵ, which is determined via equation

$$V_{ext}(\mathbf{r}, t) = \int \mathrm{d}\mathbf{r}'\mathrm{d}t' \epsilon(\mathbf{r}, \mathbf{r}', t - t') V_{tot}(\mathbf{r}', t'). \tag{25}$$

For spectroscopic applications [25] in solid state it is useful to examine these quantities in reciprocal space. In the case of periodic crystal the relevant form is $\epsilon_{\mathbf{G},\mathbf{G}'}(\mathbf{q}, \omega) = \int \mathrm{d}\mathbf{r}\mathrm{d}\mathbf{r}' \mathrm{e}^{-i(\mathbf{q}+\mathbf{G})\cdot\mathbf{r}} \mathrm{e}^{i(\mathbf{q}+\mathbf{G}')\cdot\mathbf{r}'} \epsilon(\mathbf{r}, \mathbf{r}'; \omega)$, where $\mathbf{G}$ and $\mathbf{G}'$ are reciprocal lattice vectors. The total potential in reciprocal space is then $V_{tot}(\mathbf{q} + \mathbf{G}, \omega) = \sum_{\mathbf{G}'} \epsilon^{-1}_{\mathbf{G},\mathbf{G}'}(\mathbf{q}, \omega) V_{ext}(\mathbf{q} + \mathbf{G}', \omega)$, which implies that the external perturbation creates total potential that includes other Fourier components than in the perturbation itself. If the external field is macroscopic, that is, spatially slowly varying compared to unit cell size, the total field can also contain much more rapid spatial oscillations. The occurrence of these unit-cell-scale oscillations upon macroscopic perturbation are known as local-field effects. In a completely homogeneous system the total field only contains contributions with the same $\mathbf{G}$ as the perturbing field, the local-field effects then being absent. The macroscopic potential can be obtained from a microscopic one by using an averaging

procedure that yields $V_M(\mathbf{q},\omega) = V(\mathbf{q}+\mathbf{0},\omega)$. This implies that the macroscopic total and external potentials are connected via equation $V_M^{tot}(\mathbf{q},\omega) = \epsilon^{-1}_{\mathbf{0},\mathbf{0}}(\mathbf{q},\omega)V_{ext}(\mathbf{q},\omega)$, which defines the macroscopic dielectric function as [26, 27]

$$\epsilon_M(\mathbf{q},\omega) = \frac{1}{\epsilon^{-1}_{\mathbf{0},\mathbf{0}}(\mathbf{q},\omega)}. \tag{26}$$

The macroscopic dielectric function can be cast in a convenient form in terms of modified response function $\bar{\chi}(12) = P(12) + \int \mathrm{d}(34)P(13)\bar{v}(34)\bar{\chi}(42)$, where $\bar{v}$ is a modified Coulomb interaction. In reciprocal space, $\bar{v}$ is the same as v, except in the first Brillouin zone, where it is 0. $\bar{\chi}$ can also be obtained from modified two-body correlation function $\bar{L}$, which is a solution of the BSE with v replaced with $\bar{v}$. The macroscopic dielectric function then reads [19, 28]

$$\epsilon_M(\mathbf{q},\omega) = 1 - v(\mathbf{q})\bar{\chi}_{\mathbf{0},\mathbf{0}}(\mathbf{q},\omega). \tag{27}$$

The inverse macroscopic dielectric function, on the other hand, is

$$\epsilon_M^{-1}(\mathbf{q},\omega) = 1 + v(\mathbf{q})\chi_{\mathbf{0},\mathbf{0}}(\mathbf{q},\omega). \tag{28}$$

In section 3 we see how $\epsilon_M(\mathbf{q},\omega)$ and $\epsilon_M^{-1}(\mathbf{q},\omega)$ are related to spectra that can be obtained from experiments. As χ and $\bar{\chi}$ can be inferred from L and $\bar{L}$, respectively, the connection of BSE to experimental results is then established. This connection is heavily used in paper **III**.

An important, and frequently used, approximation for the response functions is given by the random-phase approximation (RPA). For the irreducible polarizability it reads

$$P_{RPA}(\mathbf{r},\mathbf{r}';\omega) = \sum_{i,j} \phi_i^*(\mathbf{r})\phi_j(\mathbf{r})\phi_j^*(\mathbf{r}')\phi_i(\mathbf{r}') \left[\frac{f_i(1-f_j)}{\omega - (\varepsilon_j - \varepsilon_i) + i\eta} - \frac{f_j(1-f_i)}{\omega - (\varepsilon_j - \varepsilon_i) - i\eta}\right], \tag{29}$$

and it describes transitions of non-interacting electrons. η is a positive infinitesimal number that is required for the Fourier transform to be well-behaved. This form for P could then be used for subsequent calculation of χ and ϵ_M, and if the local-field effects are included, the RPA solution for ϵ_M does not describe independent e-h transitions, but the e-h exchange interaction term present in BSE is also taken into account. In paper **II** the optical absorption spectra are calculated within RPA.

2.5 Electronic excitations

A wide range of different electronic excitations can occur in materials. Excitation of a quasiparticle is one of these, and quasielectron and quasihole excitations are obtained by

adding or removing electrons from the system. Their dispersion relation in crystalline materials, that is, the energy levels as a function of wavevector $\mathbf{k}$, is known as the "electronic band structure". By the virtue of the Bloch's theorem for the many-body wavefunction, other excitations can also be assigned a crystal momentum and form band structures.

Excitons can be thought as a charge-neutral pair formed from a quasielectron and quasihole that interact via the electrostatic attraction that is screened by the other electrons (on top of the e-h exchange interaction). Excitons have often been analyzed using two models that correspond to opposing limits of localized and delocalized excitons. Frenkel excitons are localized in way that the electron and hole are found in the same building block, that can for example be atom, molecule, "super atom" [29], or atomic layer. Wannier excitons correspond to the opposing limit of large spatial extent, where the electron and hole can be far apart. These can be found in semiconductors with moderate band gap, such as silicon. Wannier excitons are often analyzed using a hydrogenic model, where the e-h attraction is screened by a dielectric constant, which can be justified when the e-h distance is large compared to distances between the atoms. Another term used to classify excitons is "charge-transfer exciton". It is sometimes thought as an intermediate case between Frenkel and Wannier excitons, in a way that the electron and hole occupy adjacent building blocks, but the definition varies and the distinction to other excitons can be ambiguous. In paper **III** any exciton where the electron and hole are in different building blocks is called charge-transfer exciton. In bulk, the exciton localization character correlates strongly with their binding energy, which can be used to distinguish different types. The Frenkel excitons have significantly larger binding energies than Wannier excitons. In two-dimensional materials this is no longer the case, as the screening is weakened by the reduced dimensionality, and also Wannier excitons spread within the plane can have large binding energies [30].

Plasmons are collective excitations that are associated with delocalized oscillations of electron density. Plasmons occur at the zeros of the $\mathrm{Re}\epsilon_{\mathrm{M}}(\mathbf{q},\omega)$ provided that the $\mathrm{Im}\epsilon_{\mathrm{M}}(\mathbf{q},\omega)$ is not too large. In fact, $\mathrm{Im}\epsilon_{\mathrm{M}}(\mathbf{q},\omega)$ provides the damping of the plasmon peak in the dynamic structure factor $S(\mathbf{q},\omega)$ (see section 3.3), and if $\mathrm{Im}\epsilon_{\mathrm{M}}(\mathbf{q},\omega)$ is large, the plasmon is said to be "merged with e-h transitions". In the case of very large $\mathrm{Im}\epsilon_{\mathrm{M}}(\mathbf{q},\omega)$ the plasmon character is eventually lost, and the excitation is better described as e-h like. In paper **III**, the relation between an exciton and a plasmon in a layered material is discussed.

3 Spectroscopic methods

3.1 Electron-photon interaction

The radiation-matter interaction can be treated either semiclassically, treating the radiation field classically and matter quantum mechanically, or by treating both radiation field and matter in the quantum theory, using the second-quantization formalism. In the fully quantum-mechanical treatment the hamiltonian describing the interaction between electrons and electromagnetic radiation is

$$H_{int} = \sum_i \left[\frac{\alpha^2}{2} \mathbf{A}^2(\mathbf{r}_i) + \alpha \mathbf{A}(\mathbf{r}_i) \cdot \mathbf{p}_i \right], \tag{30}$$

$$\mathbf{A}(\mathbf{r}) = \sum_{\mathbf{K}\lambda} \sqrt{\frac{2\pi}{\alpha^2 \mathcal{V} \omega}} \left[a(\mathbf{K},\lambda)\mathbf{e}(\mathbf{K},\lambda) \mathrm{e}^{i\mathbf{K}\cdot\mathbf{r}} + a^\dagger(\mathbf{K},\lambda)\mathbf{e}(\mathbf{K},\lambda)\mathrm{e}^{-i\mathbf{K}\cdot\mathbf{r}} \right] \tag{31}$$

where $\mathbf{A}$ is quantized vector potential, $\mathbf{p}$ electron momentum, $\mathbf{K}$ photon wavevector, a ($a^\dagger$) photon destruction (creation) operator, $\mathcal{V}$ quantization volume, $\mathbf{e}$ photon polarization, and λ index running over polarization states. By treating this interaction as a perturbation, the transition rate between the initial and final states can be obtained from the Fermi golden rule. Considering the first term in first order gives nonresonant inelastic scattering. The second-order treatment of the second term also leads to scattering, namely resonant scattering. Treating this term in first order gives photon absorption and emission. Optical absorption could then be analyzed using this formalism. Instead, in the following it is discussed in the framework of macroscopic dielectric theory, which is convenient for studying optical properties of solids [31, 32].

3.2 Optical absorption

The optical properties of crystalline materials at small $\mathbf{q}$ limit are conveniently analyzed by using macroscopic dielectric theory. This assumes that the electric field exerted on the material varies on a scale larger than the unit cell size. The field is treated classically, and the properties of the material are described quantum-mechanically by using the macroscopic dielectric tensor $\overleftrightarrow{\epsilon}_M$. It is given by the relation between the electric field $\mathbf{E}$ and the electric displacement $\mathbf{D}$:

$$\mathbf{D}(\mathbf{q},\omega) = \epsilon_0 \overleftrightarrow{\epsilon}_M(\mathbf{q},\omega)\mathbf{E}(\mathbf{q},\omega) \tag{32}$$

The vector fields $\mathbf{E}$ and $\mathbf{D}$ can be split into longitudinal and transverse components that are parallel and perpendicular to $\mathbf{q}$, respectively. Correspondingly, $\overleftrightarrow{\epsilon}_M$ is split into matrix blocks. The connection of $\overleftrightarrow{\epsilon}_M$ to the macroscopic dielectric function ϵ_M introduced in section 2.4 is that the longitudinal-longitudinal block of $\overleftrightarrow{\epsilon}_M$ is equal to

ϵ_M. In electromagnetic waves the electric field is perpendicular to the propagation of the wave, and optical absorption is determined by the transverse part of $\overleftrightarrow{\epsilon}_M$.

$\overleftrightarrow{\epsilon}_M$ is diagonal in its principal axis frame. At the optical $\mathbf{q} \to 0$ limit $\overleftrightarrow{\epsilon}_M$ is independent of direction of $\mathbf{q}$, and consequently the diagonal elements can be retrieved from the macroscopic dielectric function:

$$[\overleftrightarrow{\epsilon}_M]_i^i(\omega) = \lim_{\mathbf{q}\to 0} \epsilon_M(\mathbf{q} \| \mathbf{e}_i, \omega), \tag{33}$$

where $\mathbf{e}_i$ is the unit vector of ith coordinate axis in the principal axis frame. The dielectric tensor at $\mathbf{q} \to 0$ can hence be obtained conveniently from χ solved either from BSE or RPA.

The intensity of the electromagnetic radiation in a material attenuates according to the Beer-Lambert law $I(z) = I_0 \mathrm{e}^{-\mu(\omega)z}$, where $\mu(\omega)$ is the absorption coefficient. If the chosen sample material is irradiated with optical-wavelength electromagnetic radiation that is polarized along one of the principal axes $\mathbf{e}_i$, the electric field $\mathbf{E}$ and electric displacement $\mathbf{D}$ are parallel. Consequently, the absorption coefficient reads

$$\mu(\omega) = 2\alpha\omega\kappa(\omega), \tag{34}$$

$$\kappa(\omega) = \sqrt{\frac{\sqrt{\epsilon_1^2(\omega) + \epsilon_2^2(\omega)} - \epsilon_1(\omega)}{2}}, \tag{35}$$

where ϵ_1 and ϵ_2 are the real and imaginary parts of the diagonal element of $\overleftrightarrow{\epsilon}_M$ in equation (33). κ is the extinction coefficient that is the imaginary part of the complex refractive index $\tilde{n} = n + i\kappa$, the real part of which gives the refractive index n. The variation of κ with optical wavelengths is usually dominated by ϵ_2, and hence one often presents ϵ_2 as optical absorption spectrum, especially in theoretical work. Optical absorption spectra are discussed in papers **II** and **III**.

3.3 Inelastic x-ray scattering

The fundamental quantity measured in inelastic x-ray scattering (IXS) [33] experiments, the double differential scattering cross section (DDSCS), is related to the probability that photons with energy interval $\mathrm{d}\omega_2$ are scattered to a solid angle $\mathrm{d}\Omega$. It depends both on the photon energies of the in- and outgoing radiation fields, together with the angle of the detector and alignment of the target material. IXS experiments are often performed at synchrotron laboratories, but also new x-ray free electron lasers are being built and becoming more accessible. In the case of non-resonant inelastic x-ray scattering (NRIXS), that is, when the ingoing photon energy ω_1 is far from resonances (absorption edges) of the target material, the DDSCS can be written in the following form:

$$\frac{\mathrm{d}^2\sigma}{\mathrm{d}\Omega\ \mathrm{d}\omega} = \alpha^2 \frac{\omega_2}{\omega_1} (\mathbf{e}_1 \cdot \mathbf{e}_2)^2 S(\mathbf{q}, \omega), \tag{36}$$

$$S(\mathbf{q}, \omega) = \sum_F \left| \langle F | \sum_j \mathrm{e}^{i\mathbf{q}\cdot\mathbf{r}_j} | I \rangle \right|^2 \delta(E_I - E_F + \omega). \tag{37}$$

$|I\rangle$ and $|F\rangle$ denote initial and final states of the electron system, while $\omega = \omega_1 - \omega_2$ and $\mathbf{q} = \mathbf{K}_1 - \mathbf{K}_2$ are the energy and momentum transfer from the photon field to the electron system, respectively. $S(\mathbf{q}, \omega)$ is the dynamic structure factor, and it is purely a property of the target material. The dependence on the scattering geometry is included in the prefactor, the Thomson cross section. NRIXS can be used to probe various different electronic excitations. At the valence region, where the energy transfer is in the order of few eV, NRIXS can probe both plasmons and (screened) electron-hole-like excitations. When ω is in the vicinity of core-excitation energies, NRIXS is called x-ray Raman scattering (XRS), and it can be used as a complementary probe for x-ray absorption spectroscopy (XAS). In NRIXS, the momentum transfer can be controlled by the scattering geometry, and consequently, one can also probe nondipolar transitions in shallow absorption edges that are inaccessible via absorption spectroscopies. At the extreme limit of large energy and momentum transfer IXS is called x-ray Compton scattering, and it will be dealt in more detail in section 3.3.1.

The dynamic structure factor is linked to the electron density fluctuations in the material. It can be shown that the dynamic structure factor can be written in the form[9]

$$S(\mathbf{q}, \omega) = -\frac{1}{\pi} \mathrm{Im} \left\{ \chi_{\mathbf{0},\mathbf{0}}(\mathbf{q}, \omega) \right\} = -\frac{q^2}{4\pi^2} \mathrm{Im} \left\{ \epsilon_M^{-1}(\mathbf{q}, \omega) \right\}. \tag{38}$$

$-\mathrm{Im}\epsilon_M^{-1}(\mathbf{q}, \omega)$ is called the loss function. At the valence energy-loss region NRIXS can be used to obtain information on the dielectric function at $\mathbf{q}$ values up to several Brillouin zones. Electron energy loss spectroscopy (EELS) [34] also probes $S(\mathbf{q}, \omega)$, and can be used as a complementary tool for NRIXS.

NRIXS is related to two papers in this thesis. In paper **I** the effect of structural changes on a quantity obtainable using Compton scattering is investigated, and in paper **III** excitons and plasmons in loss function are analyzed.

3.3.1 Compton scattering

X-ray Compton scattering [35–37] is NRIXS at the limit of large energy and momentum transfer. If the momentum transfer is large enough, that is, when q^{-1} is much smaller

[9] The macroscopic dielectric function is physically meaningful concept only for macroscopic external fields. However, it enters in the theory of IXS through its mathematical connection to χ. Due to the relation between $S(\mathbf{q}, \omega)$ and ϵ_M, NRIXS can effectively be considered as a longitudinal perturbation with momentum $\mathbf{q}$ and frequency ω.

than interelectron distances, $S(\mathbf{q},\omega)$ reflects single-particle properties. If the energy transfer is very large compared to the characteristic energies of the electron system (binding energies, Fermi energy etc.), the impulse approximation is valid. According to the impulse approximation [35–38], the energy is transferred to the kinetic energy of an electron, and potential energy is the same in the initial and final states. The scattering process is so fast that electrons do not have time to rearrange before the photon has left. In mathematical terms, the impulse approximation assumes $\omega >> \sqrt{\langle I|[T,V]|I\rangle}$, where T and V are kinetic and potential energy operators, respectively. Under these conditions the dynamic structure factor can be written in the form

$$S(\mathbf{q},\omega) = \frac{1}{q}J(p_q), \tag{39}$$

$$J(p_q) = \int \mathrm{d}\mathbf{p}_\perp n(\mathbf{p} = (\mathbf{p}_\perp, p_q)), \tag{40}$$

where the integration is over a plane perpendicular to the scattering vector $\mathbf{q}$. The distance p_q of this plane from the origin is in the non-relativistic case given by the relation $p_q = \omega/q - q/2$. $n(\mathbf{p})$ is electron momentum density (EMD), and $J(p_q)$ a directional Compton profile. In isotropic systems, such as liquids, gases and powder samples, the Compton profile is isotropic as well. However, in practical calculations one can only treat a subsystem of the whole isotropic assembly and use a spherically averaged EMD $n(p)$ to calculate the isotropic Compton profile as

$$J_{iso}(p_q) = 2\pi \int_{|p_q|}^{\infty} pn(p)\mathrm{d}p, \tag{41}$$

$$n(p) = \frac{1}{4\pi}\int n(\mathbf{p})\mathrm{d}\Omega_{\mathbf{p}}, \tag{42}$$

where $\Omega_{\mathbf{p}}$ is a solid angle in momentum space. Another method to obtain the isotropic Compton profile is to calculate it as an appropriately weighted average of directional Compton profiles.

Analogous to electron density $n(\mathbf{r})$, the EMD $n(\mathbf{p})$ gives the probability to find electron with momentum $\mathbf{p}$. It can be calculated from the many-body wavefunction as

$$n(\mathbf{p}) = \frac{1}{(2\pi)^3}\int \mathrm{d}\mathbf{r}_1\mathrm{d}\mathbf{r}'_1\mathrm{e}^{-i\mathbf{p}\cdot(\mathbf{r}_1-\mathbf{r}'_1)}\int \mathrm{d}\mathbf{r}_2...\mathrm{d}\mathbf{r}_N\mathrm{d}\mathbf{r}'_2...\mathrm{d}\mathbf{r}'_N N\Phi(\mathbf{r}_1,...,\mathbf{r}_N)\Phi^*(\mathbf{r}'_1,...,\mathbf{r}'_N) \tag{43}$$

If the many-body wavefunction is given by a single Slater determinant, $n(\mathbf{p})$ reduces to a form

$$n(\mathbf{p}) = \frac{1}{(2\pi)^3} \sum_j \left| \int \mathrm{d}\mathbf{r} \mathrm{e}^{-i\mathbf{p}\cdot\mathbf{r}} \phi_j(\mathbf{r}) \right|^2 . \tag{44}$$

In paper **I** this form is used to calculate the EMD using KS orbitals as the single-particle states. The EMD in KS theory is not, however, given exactly by this equation. [39] Instead, one has include an additional term $\delta E_{xc}[n]/\delta\varepsilon_{\mathbf{p}}$, where $\varepsilon_{\mathbf{p}} = \frac{1}{2}\mathbf{p}^2$. But in practice, the simple expression (44) often gives the Compton profile difference to an accuracy [40–42] that is usable for studying structural changes.

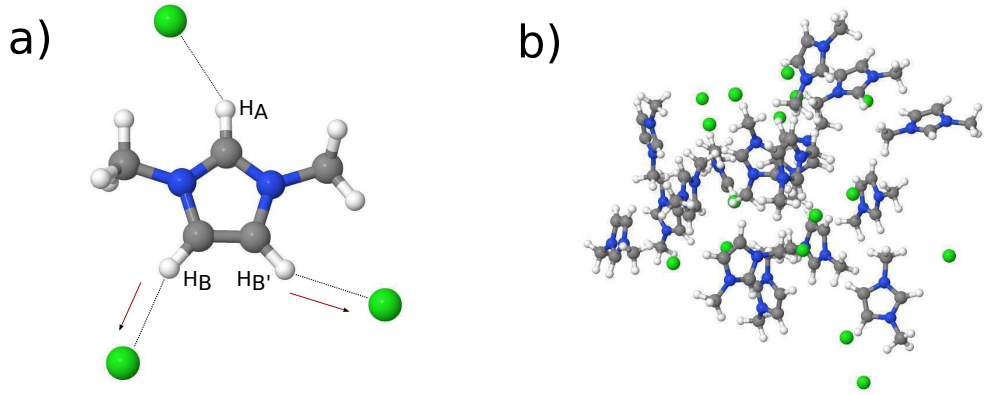

Figure 1: a) One 1,3-dimethylimidazolium molecular ion and three chloride ions. The H_A-Cl hydrogen bond on average is not changed in the phase transition, in contrast to H_B/$H_{B'}$-Cl bond whose length increases upon melting. b) A snapshot of the liquid structure.

4 Materials and questions

4.1 Ionic liquids: structure of [mmim]Cl

Usually salts, which are characterized by ionic bonding, have very large melting temperatures, for example 801° C for NaCl. Ionic liquids (ILs) [43–45], in contrast, have moderate melting temperatures, often under 100° C, even though they also exhibit ionic bonding. In ILs the ionic entities can be large, which is the origin of lower melting point. The ionic interaction is competed by other types of bonding, like hydrogen and van der Waals bonding. ILs have many useful properties, like nonflammability, nonvolatility, and thermal stability. They have attracted widespread interest both from fundamental chemistry point-of-view, and due to many possible applications, such as solvents, electrolytes, and liquid mirrors.

1,3-dimethylimidazolium chloride [mmim]Cl (see Fig. 1) is one of the simplest ionic liquids. Detailed atomic-level information on the structure of this prototype IL is of interest, since it can help to better understand the properties of this family of advanced liquids and their interaction with other components. The molecular units are small compared to many other ILs, and it could be used for benchmarking different simulation methods. Developing accurate force fields for ILs have proven to be difficult due to complex interactions. On the other hand, achieving a sufficient phase-space sampling with *ab initio* MD is challenging since large systems and time scales are required.

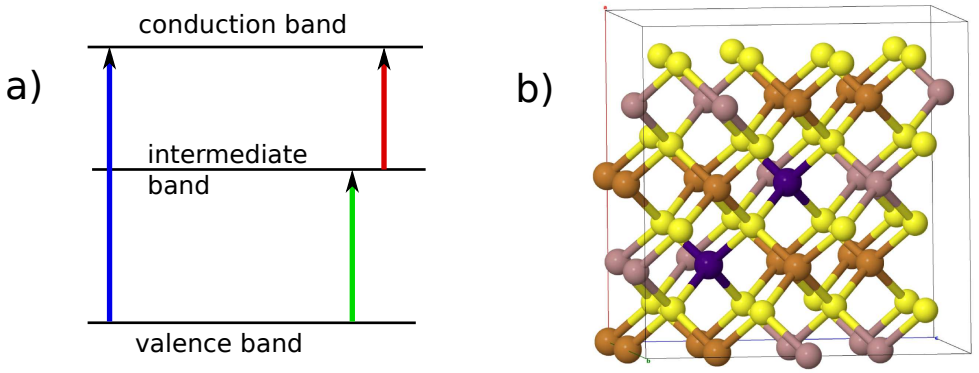

Figure 2: a) Schematic illustration of an intermediate-band solar cell. b) Supercell structure with smallest possible distance between two Fe atoms substituted on Ga site in Fe-doped $CuGaS_2$.

Previously, the structure of [mmim]Cl in liquid phase was studied using neutron scattering [46], *ab initio* MD [47–49], and classical MD [50–53]. The original motivation for modeling the Compton-profile difference in solid-liquid phase transition was to obtain information on the structure by comparing to results of an experiment performed before. However, due to complications in the experiment, the computational results were published to be compared with possible future experiments.

4.2 Fe-doped $CuGaS_2$ as an intermediate-band solar-cell material

To make photovoltaic energy conversion more affordable, there has been efforts to both make the manufacturing of solar cells cheaper and to create more efficient solar cells that convert larger part of the solar radiation energy to electricity. The efficiency can be evaluated by considering different loss mechanisms. For conventional single-band-gap solar cells the theoretical limit is known as the Shockley-Queisser limit, in which case the 31 % of the radiation energy under one sun illumination can be converted to electricity. To go beyond this limit, that is, to manufacture so-called third generation solar cells [54, 55], one has to circumvent at least one of the hindrances inherent to these conventional cells.

One of the assumptions in the Shockley-Queisser limit is that the electron and hole drift to conduction band minimum and valence band maximum, respectively, before being collected. This is a result of scattering with phonons, and the photon energy exceeding the band gap is lost to thermal vibrations. Another limiting factor is that

photons with energy smaller than the band gap are not harvested. One way to go around these problems is to engineer additional states in the band gap, which can significantly improve the efficiency. These additional bands are called intermediate bands (IBs); see Fig 2a for a schematic illustration. There can be a single IB localized in energy, or several IBs spread over the gap. Compared to empty IB, a single IB is more efficient when it is half filled; then there are more electrons to be excited from IB to conduction band. Of course, empty IBs could also be exploited, but the photocurrent created this way is significantly smaller as two subsequent photon absorption events are required.

Intermediate-band solar cells [56–58] can be realized by quantum dots, and doped semiconductors. The approach by doping semiconductors has been studied with several dopants and host semiconductor materials. $CuGaS_2$ is a one candidate for a host semiconductor, and it has a band gap close to the optimal value for a single half-filled IB [59]. For $CuGaS_2$, several dopants have been theoretically studied [60–73], while in the case of Fe an actual solar-cell device has also been built [74]. Due to this, Fe-doped $CuGaS_2$ was chosen for a theoretical study in order to obtain information on its atomic-level and band structure to explain the origin of its properties. An example structure used in calculations is shown in Fig 2b.

In optical absorption experiments [74, 75] two broad sub-band-gap peaks were observed at 1.2 and 1.9 eV. In a previous work [75] both of these peaks were assigned to Fe $3d$ derived levels, the 1.2 lower peak to crystal-field resonance e^{CFR} states, and 1.9 eV peak to dangling-bong hybrid t_2^{DBH} states. However, accurate first-principles calculations on the nature of the IBs are of interest to further shed light on this issue, and in paper **II** this task is approached using hybrid-functional calculations.

4.3 Hexagonal boron nitride: excitons in layered materials

Layered materials have attracted a lot of attention in recent years [76–79] and prospects are hold for using them in electronic devices, for example. These materials consist of one-atom-thin layers that are bound together by weak van der Waals forces. Their properties can be modified by stacking different kind of layers, which allows engineering devices with desired functionality. For optoelectronic applications, the excitons in these materials are of crucial importance. It is hence very useful to understand the exciton properties from the knowledge of the two-dimensional building blocks and their properties, which is the main aim of paper **III**.

Hexagonal boron nitride (hBN) is a wide-gap insulator that has been studied much in recent years. It is a layered material formed of boron nitride single layers (see figure 3). The calculated indirect quasiparticle gap is around 5.8 eV, while the direct gap is about 0.7 eV larger (in paper **III**). The lowest excitons are strongly bound on the basis of first-principles BSE calculations [80–84], with an exciton binding energy around

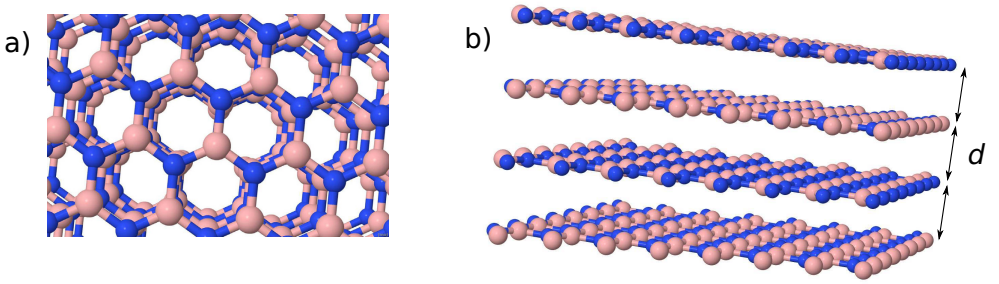

Figure 3: a) The structure of hexagonal boron nitride (hBN) from above, looking perpendicular to the planes. b) Sideview of the same structure. By increasing the interlayer distance d, one can modify the effects of interlayer hopping and exchange electron-hole interaction.

0.7 eV in bulk. These excitons can be considered as Frenkel excitons formed from "super atoms" that consists of few atoms. When going from bulk to single layer, the optical absorption energy is almost unchanged. This does not imply that the exciton binding energy stays the same, but rather that the increase of quasiparticle gap is cancelled by the increase of exciton binding energy. Besides optical $\mathbf{q} \to 0$ limit, first-principles calculations have been able to describe the dielectric function in a wide range of momentum and energy by comparison to NRIXS experiments [85].

Even though hBN is a material of interest in itself, it is chosen for this study because its exciton properties are well studied with first-principles calculations, and it can be thought as prototypical layered material for studying exciton properties. The numerical BSE results calculated in paper **III** are used to compare to model calculations that are of general validity. The model developed in paper **III** for layered systems is based on previous models used on molecular solids [86–88] and single layer materials [30]. One can then describe properties of layered materials based on properties of single layer. By changing the interlayer distance one can modify the interlayer hopping (which gives rise to band dispersion), and study how it affects exciton dispersion. In general, the effect of hopping is to mix Frenkel and charge-transfer excitons.

5 Results and discussion

5.1 Paper I: Intra- and intermolecular effects on the Compton profile of the ionic liquid 1,3-dimethylimidazolium chloride

In this work, liquid and solid-state structures were obtained using *ab initio* MD simulations and the difference profile $\Delta J(p_q) = J_{liquid} - J_{solid}$ was subsequently calculated using KS DFT. The structural changes that give rise to the difference profile were then analyzed in detail.

To compare the used liquid structures with the results of the previous works the partial radial distribution functions (RDFs) were analyzed. The RDFs were in overall good agreement to previously published [47–49], although some differences were found, as also among previous results. The solid-state structures were obtained first by geometry optimizing the structure obtained from x-ray diffraction [89], and then starting *ab initio* MD from the geometry-optimized structure. The MD simulations for solid state were done in order to take the effects of vibrations into account. It was found that the intramolecular mean bond lengths from MD were systematically longer than in the geometry-optimized structure. Even though this vibrational effect might first seem quite small, it had a significant effect on the difference profile, as Compton scattering is very sensitive to changes in intramolecular bonds.

The resulting difference profile was dominated by intermolecular changes. This can be seen in that the difference profile quite well resembles a damped oscillation with a period characteristic to intermolecular changes. In contrast, if geometry-optimized structure for solid is used, the difference profile also has significant contribution from intramolecular changes, and the shape of ΔJ is clearly different. By looking at the studied bond length changes, one can hypothesize that the elongation of the hydrogen bonds of the two neighboring ring hydrogens (see Fig. 1a) play a major role in the difference profile. Of course, there can also be important structural changes that are not fully captured in the presented bond length distributions and their mean values.

5.2 Paper II: First-principles analysis of the intermediate band in $\mathbf{CuGa_{1-x}Fe_xS_2}$

To gain insight on the structural configurations of the Fe impurities in $GuGaS_2$ and their effects on electronic structure, 4 different supercell structures of 64 atoms that include 2 Fe dopants were studied, following Ref. [60]. It was found that the structure with the shortest distance between the impurities (S-CGS:Fe) was energetically most preferred. Furthermore, antiferromagnetic ordering of the dopants was favored for all structures, most for the S-CGS:Fe. As the antiferromagnetic S-CGS:Fe had clearly

the dominating probability in thermal equilibrium, it was chosen for more detailed calculations. The tendency of impurities to cluster was further studied using 128-atom cells with 4 Fe dopants. The cell where the 4 impurities were closest was indeed energetically preferred to others. However, one should keep in mind that the structure of real sample materials may depend on the preparation.

The IBs in S-CGS:Fe were located 1.6-1.9 eV above the valence band maximum (VBM) and were unoccupied. These IBs predominantly derived from the empty $3d$ orbitals of Fe. The dopant had only a negligible effect on the band gap of $CuGaS_2$. Interestingly, the band structure is qualitatively different when calculated using semilocal PBE functional: the IBs that were very close to each other split to 2 separated structures.

The optical absorption spectra were calculated using RPA. Although the absorption onset was around 1.6 eV that corresponds to the distance between VBM and IB, the first absorption peak was clearly above 2 eV. This is a result of neglecting the excitonic effects, which besides creating bound excitons also shift spectral weight to lower energies by modifying the oscillator strengths of the transitions. As the used HSE functional has tendency to underestimate band gap in $CuGaS_2$ it is quite natural to ascribe the IBs found in this work to the 1.9 eV peak found in experiments. It is then tempting to assign the 1.2 eV feature to some additional defect structure that was not taken into account in this work. However, transition-metal-doped semiconductors are challenging systems to model (see Ref. 90, for example), and it is not obvious that the used functional can completely describe the band structure in this system. Furthermore, structural effects around substitutional Fe may modify the positions of Fe $3d$ derived energy levels leading to larger separation between them.

The IB solar cell can work more efficiently when the IB is partially filled, but the IBs in our work were empty. For this reason, we studied the possibility to partially fill the IBs by adding electrons that could in principle be provided by n-type co-doping. We found that filled bands in the gap could only be obtained by moderate concentrations of added electrons. By increasing the concentration, filled IBs shifted towards VBM, and eventually coalesced with the valence band.

5.3 Paper III: Excitons in van der Waals materials: from monolayer to bulk hexagonal boron nitride

The calculated optical absorpion spectra in bulk hBN are generally in good agreement with previous BSE calculations [80–84]. The first visible exciton (denoted "A^+") is degenerate to a dark one (denoted "B^+"), and below these there are two dark excitons (that is, excitons that have zero oscillator strength and are not visible in spectrum) that are denoted as "A^-" and "B^-". The loss function at $\mathbf{q} \to 0$ has its first visible peak around 6 eV, which is a plasmon that resides below the quasiparticle gap due to

strong excitonic effects.

Interesting changes start to occur at finite momentum transfer[10] $\mathbf{q}$. Most importantly, A^- becomes visible. This exciton first shows as a small prepeak below A^+, but grow with $\mathbf{q}$ finally even becoming higher than A^+. The excitons disperse in $\mathrm{Im}\epsilon_\mathrm{M}(\mathbf{q},\omega)$ in increasing energy order as B^-, A^-, B^+, A^+, while in loss function excitons dispersing similarly to the 3 lowest ones can be observed. To study the effect of exchange e-h interaction the spectra were also calculated for the spin triplet, where the v term that gives rise to the exchange e-h interaction is absent. The excitons disperse in same order, but the dispersion is significanly tempered for A^- (and to lesser extent A^+), which means that the exchange e-h interaction is important for it.

To better reveal the role of interlayer hopping and e-h exchange interaction, the corresponding results were calculated with the interlayer distance d increased to 1.5 times the bulk value d_0. At this d, the interlayer dispersion is significantly reduced and bands are nearly flat in the direction perpendicular to the monolayer plane. In $\mathrm{Im}\epsilon_\mathrm{M}(\mathbf{q},\omega)$ all the excitons become practically degenerate at $\mathbf{q}\to 0$ and A^- is dark at all $\mathbf{q}$ implying that hopping plays an important role in its visibility in bulk phase. A^- does however disperse very strongly, and is on higher energy than A^+, while B^- and B^+ are on lower energy and degenerate to each other. In triplet, all the 4 excitons are almost degenerate at all momenta, and their dispersion is very similar to B^- and B^+ in $\mathrm{Im}\epsilon_\mathrm{M}(\mathbf{q},\omega)$. This implies that the exchange e-h interaction is insignificant for B^- and B^+ but is important for A^- and A^+. The dispersion of these excitons in loss function is similar to $\mathrm{Im}\epsilon_\mathrm{M}(\mathbf{q},\omega)$, except that A^+ is absent. The plasmon approaches A^- at large $\mathbf{q}$, and as also A^+ in $\mathrm{Im}\epsilon_\mathrm{M}(\mathbf{q},\omega)$ approaches A^- (this is more evident for $d > 1.5d_0$), this hints that the plasmon may be related to A^+.

The changes in the spectra at finite $\mathbf{q}$ and at increased d are very well explained by the model that is derived from BSE by utilizing wavefunctions localized in the planes. The "A" and "B" in the peak labels actually derive from labelling of the excitons in the monolayer, while "+" and "-" refer to excitons symmetric and antisymmetric in the change of e-h pairs in the two layers of the unit cell. This assignment originates from the nature of Frenkel excitons[11] in the layered materials. When the interlayer hopping is taken into account, the "+" and "-" excitons mix, as also Frenkel and charge-transfer excitons do. However, the label names (A^+ etc.) are still used for bulk where interlayer hopping is significant.

The reason why B^- and B^+ are dark follows from the fact the B exciton in monolayer is dark as well. The in-plane dipole matrix element that gives the visibility also determines the exchange e-h interaction in monolayer, so that B exciton does not feel it. Correspondingly, this dipole matrix element shows in the prefactor of exchange e-h

[10] The momentum transfer in this study is in ΓM direction in the plane

[11] Here, Frenkel exciton refers to an exciton where electron and hole are in the same layer, regardless of the separation within the layer.

interaction in bulk, which explains why B^- and B^+ are not affected by this interaction. The A exciton in monolayer has a finite dipole matrix element and is visible, and consequently A^+ is visible without hopping. A^- is dark without hopping because equal terms cancel in the dipole matrix element. The hopping allows the negative-parity state to mix with positive-parity ones at finite $\mathbf{q}$, which explains why A^- becomes visible in bulk at finite momenta. The fact that both A^- and A^+ feel the exchange e-h interaction is also traced back to the finite dipole matrix element of monolayer A exciton. By using the model one can find that the plasmon can really be associated with the A^+ exciton. Including the long-range term absent in $\bar{v}$ shifts the energy of the A^+ exciton upwards so that it may be assimilated with the plasmon. Indeed, the plasmon energy in loss function and the A^+ exciton energy approach each other when $\mathbf{q}$ is increased, faster the larger d is ($\mathrm{Im}\epsilon_{\mathrm{M}}(\mathbf{q},\omega)$ and loss function coincide when $\mathbf{q} \to \infty$ or $d \to \infty$).

6 Concluding remarks

This thesis included applications of electronic-structure calculations in three different research projects, and their topics span a wide range from structure of complex liquids to theory of excitons. However, all of these papers had in common that they were related to response of matter to electromagnetic radiation, from absorption of visible light to scattering of hard x rays.

A prediction of Compton difference profile in solid-to-liquid phase transition was presented to be compared with future experiments. The liquid structure and structural changes in the phase transition were analyzed to understand which effects give rise to the predicted signal. The nature of intermediate-band states in Fe-doped $CuGaS_2$ was studied, and the results were discussed in relation to previous optical absorption experiments. Exciton dispersion in a prototypical layered insulator hexagonal boron nitride was investigated, and first-principles results were analyzed in terms of interlayer hopping and exchange e-h interaction, and connection to excitons of monolayer was discussed.

In future, both the increase of computational power and progress in theory and codes will lead to interesting developments in the field. Accurate many-body methods become available to more and more complex systems. The Bethe-Salpeter equation may become a standard method of predicting optical response in systems of great complexity, including realistic doped structures, for example. Also, improved accuracy in first-principles calculations in systems with localized electrons is of significant interest.

References

[1] R. M. Martin, *Electronic structure: basic theory and practical methods* (Cambridge university press, 2004).

[2] T. Helgaker, P. Jorgensen, and J. Olsen, *Molecular electronic-structure theory* (John Wiley & Sons, 2014).

[3] P. Hohenberg and W. Kohn, *Inhomogeneous Electron Gas*, Phys. Rev. **136**, B864 (1964).

[4] *A primer in density functional theory*, edited by C. Fiolhais, F. Nogueira, and M. A. Marques (Springer Science & Business Media, 2003), Vol. 620.

[5] K. Capelle, *A bird's-eye view of density-functional theory*, Braz. J. Phys. **36**, 1318 (2006).

[6] M. Levy, *Universal variational functionals of electron densities, first-order density matrices, and natural spin-orbitals and solution of the v-representability problem*, Proc. Natl. Acad. Sci. U.S.A. **76**, 6062 (1979).

[7] W. Kohn and L. J. Sham, *Self-Consistent Equations Including Exchange and Correlation Effects*, Phys. Rev. **140**, A1133 (1965).

[8] C.-O. Almbladh and U. von Barth, *Exact results for the charge and spin densities, exchange-correlation potentials, and density-functional eigenvalues*, Phys. Rev. B **31**, 3231 (1985).

[9] A. Seidl, A. Görling, P. Vogl, J. Majewski, and M. Levy, *Generalized Kohn-Sham schemes and the band-gap problem*, Phys. Rev. B **53**, 3764 (1996).

[10] A. D. Becke, *A new mixing of Hartree–Fock and local density-functional theories*, J. Chem. Phys. **98**, 1372 (1993).

[11] J. P. Perdew, M. Ernzerhof, and K. Burke, *Rationale for mixing exact exchange with density functional approximations*, J. of Chem. Phys. **105**, 9982 (1996).

[12] L. Hedin, *New method for calculating the one-particle Green's function with application to the electron-gas problem*, Phys. Rev. **139**, A796 (1965).

[13] A. Alkauskas, P. Broqvist, and A. Pasquarello, *Defect levels through hybrid density functionals: Insights and applications*, Phys. Status Solidi B **248**, 775 (2011).

[14] M. A. Marques, J. Vidal, M. J. Oliveira, L. Reining, and S. Botti, *Density-based mixing parameter for hybrid functionals*, Phys. Rev. B **83**, 035119 (2011).

[15] J. Heyd, G. E. Scuseria, and M. Ernzerhof, *Hybrid functionals based on a screened Coulomb potential*, J. Chem. Phys. **118**, 8207 (2003).

[16] J. Heyd, G. E. Scuseria, and M. Ernzerhof, *Erratum:"Hybrid functionals based on a screened Coulomb potential"[J. Chem. Phys. 118, 8207 (2003)]*, J. Chem. Phys. **124**, 219906 (2006).

[17] J. Paier, M. Marsman, K. Hummer, G. Kresse, I. C. Gerber, and J. G. Ángyán, *Screened hybrid density functionals applied to solids*, J. Chem. Phys. **124**, 154709 (2006).

[18] G. Strinati, *Application of the Green's functions method to the study of the optical properties of semiconductors*, Rivista del Nuovo Cimento **11**, 1 (1988).

[19] G. Onida, L. Reining, and A. Rubio, *Electronic excitations: density-functional versus many-body Green's-function approaches*, Rev. Mod. Phys. **74**, 601 (2002).

[20] R. M. Martin, L. Reining, and D. M. Ceperley, *Interacting Electrons: Theory and Computational Approaches* (Cambridge University Press, 2016).

[21] R. D. Mattuck, *A guide to Feynman diagrams in the many-body problem* (Courier Corporation, 2012).

[22] A. L. Fetter and J. D. Walecka, *Quantum theory of many-particle systems* (Courier Corporation, 2003).

[23] R. Haydock, *The recursive solution of the Schrödinger equation*, Comput. Phys. Commun. **20**, 11 (1980).

[24] M. Grüning, A. Marini, and X. Gonze, *Implementation and testing of Lanczos-based algorithms for random-phase approximation eigenproblems*, Comput. Mater. Sci. **50**, 2148 (2011).

[25] S. Botti and M. Gatti, *Fundamentals of time-dependent density functional theory* (Springer, 2012), pp. 29–50.

[26] S. L. Adler, *Quantum theory of the dielectric constant in real solids*, Phys. Rev. **126**, 413 (1962).

[27] N. Wiser, *Dielectric constant with local field effects included*, Phys. Rev. **129**, 62 (1963).

[28] W. Hanke, *Dielectric theory of elementary excitations in crystals*, Adv. Phys. **27**, 287 (1978).

[29] P. Abbamonte, T. Graber, J. P. Reed, S. Smadici, C.-L. Yeh, A. Shukla, J.-P. Rueff, and W. Ku, *Dynamical reconstruction of the exciton in LiF with inelastic x-ray scattering*, Proc. Nat. Acad. Sci. **105**, 12159 (2008).

[30] P. Cudazzo, L. Sponza, C. Giorgetti, L. Reining, F. Sottile, and M. Gatti, *Exciton band structure in two-dimensional materials*, Physical Rev. Lett. **116**, 066803 (2016).

[31] M. Fox, *Optical properties of solids* (Oxford university press, 2010), Vol. 3.

[32] F. Wooten, *Optical properties of solids* (Academic press, 2013).

[33] W. Schülke, *Electron dynamics by inelastic X-ray scattering* (Oxford University Press, 2007).

[34] R. F. Egerton, *Electron energy-loss spectroscopy in the electron microscope* (Springer Science & Business Media, 2011).

[35] *X-ray Compton scattering*, edited by M. Cooper, P. Mijnarends, N. Shiotani, N. Sakai, and A. Bansil (Oxford University Press, 2004).

[36] M. J. Cooper, *Compton scattering and electron momentum determination*, Rep. Prog. Phys. **48**, 415 (1985).

[37] *Compton scattering: the investigation of electron momentum distributions*, edited by B. Williams (McGraw-Hill, 1977).

[38] I. Kaplan, B. Barbiellini, and A. Bansil, *Compton scattering beyond the impulse approximation*, Phys. Rev. B **68**, 235104 (2003).

[39] L. Lam and P. Platzman, *Momentum density and Compton profile of the inhomogeneous interacting electronic system. I. Formalism*, Phys. Rev. B **9**, 5122 (1974).

[40] T. K. Ghanty, V. N. Staroverov, P. R. Koren, and E. R. Davidson, *Is the Hydrogen Bond in Water Dimer and Ice Covalent?*, J. Am. Chem. Soc. **122**, 1210 (2000).

[41] M. Hakala, S. Huotari, K. Hämäläinen, S. Manninen, P. Wernet, A. Nilsson, and L. G. M. Pettersson, *Compton profiles for water and mixed water-neon clusters: A measure of coordination*, Phys. Rev. B **70**, 125413 (2004).

[42] J. Lehtola, M. Hakala, J. Vaara, and K. Hämäläinen, *Calculation of isotropic Compton profiles with Gaussian basis sets*, Phys. Chem. Chem. Phys. **13**, 5630 (2011).

[43] A. Pinkert, K. Marsh, S. Pang, and M. Staiger, *Ionic Liquids and Their Interaction with Cellulose*, Chem. Rev. **109**, 6712 (2009).

[44] J. Hallet and T. Welton, *Room-Temperature Ionic Liquids: Solvents for Synthesis and Catalysis. 2*, Chem. Rev. **111**, 3508 (2011).

[45] E. W. Castner Jr and J. F. Wishart, *Spotlight on ionic liquids*, J. Chem. Phys. **132**, 120901 (2010).

[46] C. Hardacre, J. D. Holbrey, S. E. J. McMath, D. T. Bowron, and A. K. Soper, *Structure of molten 1,3-dimethylimidazolium chloride using neutron diffraction*, J. Chem. Phys. **118**, 273 (2003).

[47] M. G. Del Pópolo, R. M. Lynden-Bell, and J. Kohanoff, *Ab Initio Molecular Dynamics Simulation of a Room Temperature Ionic Liquid*, J. Phys. Chem. B **109**, 5895 (2005).

[48] M. Buhl, A. Chaumont, R. Schurhammer, and G. Wipff, *Ab Initio Molecular Dynamics of Liquid 1,3-dimethylimidazolium Chloride*, J. Phys. Chem. B **109**, 18591 (2005).

[49] B. L. Bhargava and S. Balasubramanian, *Intermolecular structure and dynamics in an ionic liquid: A Car–Parrinello molecular dynamics simulation study of 1,3-dimethylimidazolium chloride*, Chem. Phys. Lett. **417**, 486 (2006).

[50] B. L. Bhargava and S. Balasubramanian, *Dynamics in a room-temperature ionic liquid: A computer simulation study of 1,3-dimethylimidazolium chloride*, J. Chem. Phys. **123**, 144505 (2005).

[51] B. L. Bhargava and S. Balasubramanian, *Erratum: "Dynamics in a room temperature ionic liquid: A computer simulation study of 1,3-dimethylimidazolium chloride" [J. Chem. Phys.123, 144505 (2005)]*, J. Chem. Phys. **125**, 219901 (2006).

[52] T. G. A. Youngs, M. G. Del Pópolo, and J. Kohanoff, *Development of Complex Classical Force Fields through Force Matching to ab Initio Data: Application to a Room-Temperature Ionic Liquid*, J. Phys. Chem. B **110**, 5697 (2006).

[53] S. M. Urahata and M. C. C. Rebeiro, *Structure of ionic liquids of 1-alkyl-3-methylimidazolium cations: A systematic computer simulation study*, J. Chem. Phys. **120**, 1855 (2004).

[54] G. Conibeer, *Third-generation photovoltaics*, Materials today **10**, 42 (2007).

[55] M. A. Green, *Third generation photovoltaics* (Springer, 2006).

[56] A. Luque and A. Martí, *Increasing the efficiency of ideal solar cells by photon induced transitions at intermediate levels*, Phys. Rev. Lett. **78**, 5014 (1997).

[57] A. Luque, A. Martí, and C. Stanley, *Understanding intermediate-band solar cells*, Nat. Photon. **6**, 146 (2012).

[58] Y. Okada, N. Ekins-Daukes, T. Kita, R. Tamaki, M. Yoshida, A. Pusch, O. Hess, C. Phillips, D. Farrell, K. Yoshida, *et al.*, *Intermediate band solar cells: Recent progress and future directions*, Appl. Phys. Rev. **2**, 021302 (2015).

[59] A. Martí, D. F. Marrón, and A. Luque, *Evaluation of the efficiency potential of intermediate band solar cells based on thin-film chalcopyrite materials*, J. Appl. Phys. **103**, 073706 (2008).

[60] J. Hashemi, A. Akbari, S. Huotari, and M. Hakala, *Multi-intermediate-band character of Ti-substituted CuGaS 2: Implications for photovoltaic applications*, Phys. Rev. B **90**, 075154 (2014).

[61] M. Han, X. Zhang, and Z. Zeng, *The investigation of transition metal doped CuGaS 2 for promising intermediate band materials*, RSC Adv. **4**, 62380 (2014).

[62] P. Chen, M. Qin, H. Chen, C. Yang, Y. Wang, and F. Huang, *Cr incorporation in CuGaS2 chalcopyrite: A new intermediate-band photovoltaic material with wide-spectrum solar absorption*, Phys. Status Solidi A **210**, 1098 (2013).

[63] C. Yang, M. Qin, Y. Wang, D. Wan, F. Huang, and J. Lin, *Observation of an intermediate band in Sn-doped chalcopyrites with wide-spectrum solar response*, Sci. Rep. **3**, 1286 (2013).

[64] Y. Seminóvski, P. Palacios, and P. Wahnón, *Intermediate band position modulated by Zn addition in Ti doped CuGaS 2*, Thin Solid Films **519**, 7517 (2011).

[65] C. Tablero and D. Fuertes Marrón, *Analysis of the electronic structure of modified CuGaS2 with selected substitutional impurities: prospects for intermediate-band thin-film solar cells based on Cu-containing chalcopyrites*, J. Phys. Chem. C **114**, 2756 (2010).

[66] C. Tablero, *Electronic and optical properties of the group IV doped copper gallium chalcopyrites*, Thin Solid Films **519**, 1435 (2010).

[67] I. Aguilera, P. Palacios, and P. Wahnón, *Enhancement of optical absorption in Ga-chalcopyrite-based intermediate-band materials for high efficiency solar cells*, Sol. Energ. Mat. Sol. Cells **94**, 1903 (2010).

[68] I. Aguilera, P. Palacios, and P. Wahnón, *Optical properties of chalcopyrite-type intermediate transition metal band materials from first principles*, Thin Solid Films **516**, 7055 (2008).

[69] P. Palacios, I. Aguilera, P. Wahnón, and J. C. Conesa, *Thermodynamics of the formation of Ti-and Cr-doped CuGaS2 intermediate-band photovoltaic materials*, J. Phys. Chem. C **112**, 9525 (2008).

[70] P. Palacios, K. Sánchez, J. Conesa, J. Fernández, and P. Wahnón, *Theoretical modelling of intermediate band solar cell materials based on metal-doped chalcopyrite compounds*, Thin Solid Films **515**, 6280 (2007).

[71] P. Palacios, K. Sánchez, J. Conesa, and P. Wahnón, *First principles calculation of isolated intermediate bands formation in a transition metal-doped chalcopyrite-type semiconductor*, Phys. Status Solidi A **203**, 1395 (2006).

[72] Z. Zongyan, Z. Dacheng, and Y. Juan, *Analysis of the electronic structures of 3d transition metals doped CuGaS2 based on DFT calculations*, J. Semicond. **35**, 013002 (2014).

[73] M. Han, X. Zhang, Y. Zhang, and Z. Zeng, *The group VA element non-compensated n–p codoping in CuGaS 2 for intermediate band materials*, Sol. Energ. Mat. Sol. Cells **144**, 664 (2016).

[74] B. Marsen, S. Klemz, T. Unold, and H.-W. Schock, *Investigation of the Sub-Bandgap Photoresponse in CuGaS2: Fe for Intermediate Band Solar Cells*, Prog. Photovolt: Res. Appl. **20**, 625 (2012).

[75] K. Tanaka, K. Ishii, S. Matsuda, Y. Hasegawa, and K. Sato, *Optical characterization of deep levels in single crystals of CuGaS2 grown by chemical vapor transport*, Jpn. J. Appl. Phys. **28**, 12 (1989).

[76] F. Xia, H. Wang, D. Xiao, M. Dubey, and A. Ramasubramaniam, *Two-dimensional material nanophotonics*, Nature Photonics **8**, 899 (2014).

[77] A. K. Geim and I. V. Grigorieva, *Van der Waals heterostructures*, Nature **499**, 419 (2013).

[78] G. R. Bhimanapati, Z. Lin, V. Meunier, Y. Jung, J. Cha, S. Das, D. Xiao, Y. Son, M. S. Strano, V. R. Cooper, *et al.*, *Recent advances in two-dimensional materials beyond graphene*, Acs Nano **9**, 11509 (2015).

[79] S. Z. Butler, S. M. Hollen, L. Cao, Y. Cui, J. A. Gupta, H. R. Gutierrez, T. F. Heinz, S. S. Hong, J. Huang, A. F. Ismach, *et al.*, *Progress, challenges, and opportunities in two-dimensional materials beyond graphene*, ACS nano **7**, 2898 (2013).

[80] L. Wirtz, A. Marini, M. Grüning, and A. Rubio, *Excitonic effects in optical absorption and electron-energy loss spectra of hexagonal boron nitride*, arXiv:cond-mat/0508421 (2005).

[81] B. Arnaud, S. Lebègue, P. Rabiller, and M. Alouani, *Huge Excitonic Effects in Layered Hexagonal Boron Nitride*, Phys. Rev. Lett. **96**, 026402 (2006).

[82] L. Wirtz, A. Marini, and A. Rubio, *Excitons in Boron Nitride Nanotubes: Dimensionality Effects*, Phys. Rev. Lett. **96**, 126104 (2006).

[83] L. Wirtz, A. Marini, M. Grüning, C. Attaccalite, G. Kresse, and A. Rubio, *Comment on "Huge Excitonic Effects in Layered Hexagonal Boron Nitride"*, Phys. Rev. Lett. **100**, 189701 (2008).

[84] B. Arnaud, S. Lebègue, P. Rabiller, and M. Alouani, *Arnaud, Lebègue, Rabiller, and Alouani Reply:*, Phys. Rev. Lett. **100**, 189702 (2008).

[85] G. Fugallo, M. Aramini, J. Koskelo, K. Watanabe, T. Taniguchi, M. Hakala, S. Huotari, M. Gatti, and F. Sottile, *Exciton energy-momentum map of hexagonal boron nitride*, Phys. Rev. B **92**, 165122 (2015).

[86] P. Cudazzo, M. Gatti, and A. Rubio, *Excitons in molecular crystals from first-principles many-body perturbation theory: picene versus pentacene*, Phys. Rev. B **86**, 195307 (2012).

[87] P. Cudazzo, M. Gatti, A. Rubio, and F. Sottile, *Frenkel versus charge-transfer exciton dispersion in molecular crystals*, Phys. Rev. B **88**, 195152 (2013).

[88] P. Cudazzo, F. Sottile, A. Rubio, and M. Gatti, *Exciton dispersion in molecular solids*, J. Phys. Condens. Matter **27**, 113204 (2015).

[89] A. Arduengo, H. Dias, R. Harlow, and M. Kline, *Electronic Stabilization of Nucleophilic Carbenes*, J. Am. Chem. Soc. **114**, 5530 (1992).

[90] V. Ivády, I. Abrikosov, E. Janzén, and A. Gali, *Role of screening in the density functional applied to transition-metal defects in semiconductors*, Phys. Rev. B **87**, 205201 (2013).